2022-12-01

Fabrication, Microstructure And Mechanical Characterization of CrVNbTaW High Entropy Alloy Coatings Using Magnetron Sputtering

Jorge Quezada
University of Texas at El Paso

FABRICATION, MICROSTRUCTURE AND MECHANICAL CHARACTERIZATION OF CrVNbTaW HIGH ENTROPY ALLOY COATINGS USING MAGNETRON SPUTTERING

JORGE ESDING QUEZADA

Master's Program in Mechanical Engineering

APPROVED:

Chintalapalle Ramana, Ph.D., Chair

Barry Benedict, Ph.D.

Methaq Abed, Ph.D.

Das Debabratha, Ph.D

Stephen L. Crites, Jr., Ph.D.
Dean of the Graduate School

Dedication

To all the people I love.

FABRICATION, MICROSTRUCTURE AND MECHANICAL CHARACTERIZATION OF CrVNbTaW HIGH ENTROPY ALLOY COATINGS USING MAGNETRON SPUTTERING

by

JORGE ESDING QUEZADA

Presented to the Faculty of the Graduate School of

The University of Texas at El Paso

in Partial Fulfillment

of the Requirements

for the Degree of

MASTER OF SCIENCE

Department of Mechanical Engineering

THE UNIVERSITY OF TEXAS AT EL PASO

December 2022

Acknowledgements

Big thanks to everyone who has been a part of my journey.

Abstract

In this project a CrVNbTaW high entropy alloy was evaluated. The samples were made using radio frequency magnetron sputtering and were made under similar conditions. The deposition parameters were explored to find the ideal deposition process. The process included a pressure from 0.1-2mTorr, 600C, 1 hour duration, at 100W power to guns, and constant argon flow. The samples were fabricated under similar parameters using silicon steel and sapphire substrates. The samples were analyzed and characterized using X-ray diffraction, scanning electron microscopy, atomic force microscopy, nanoindentation and corrosion testing. Based on these results we were able to

Table of Contents

List of Tables

List of Figures

Chapter 1: Introduction

Metals are some of the most useful materials in the world all throughout the bronze, iron and now steel ages. Since metals are very useful for many different things much research has gone into developing new ways and methods of maximizing the life and usage of these metals. When metals are mixed with other metals this creates an alloy which can have various different desirable properties.[1-3]

These different attractive properties have caused high entropy alloys (HEA's) to be a promising area of research. HEA's can have high temperature resistance, high strain rate, increased hardness levels and anticorrosive qualities which have applications from high temperature bearing structures, hard coatings to military armor.[3-6] Although there is not a common overall definition for high entropy alloys according to Zhang et al HEA's can be defined as "alloys containing at least 5 principal elements, each with an atomic percentage (at. %) between 5% and 35%." [3]

HEA's are complex for the reason that they have many different intermetallic and intermediate phases.[1] These numerous phases can at times have a desirable effect that can be useful for a number of reasons. This myriad of different so called micro combinations of the metals that formed within these alloys is very difficult to quantify and is barely at its infancy in terms of researching these massive matrixes. There are many parameters which play into the formation of an HEA coating on a surface which include the atomic sizes, mixing enthalpy, concentration of valence electrons and electronegativities.[1] Considering the 5 different elements used there are many different combinations which could potentially form.

Since around 2004 there has been extensive investigation into various compositions of these high entropy alloys. Huang et al explain there are 4 core effects which come into play in the

formation of microstructure of this composition and therefore influences the properties of this HEA. These are the high entropy effect, sluggish diffusion effect, severe lattice distortion effect, and cocktail effect.[5]

First, is the high entropy effect which involves the 2nd law of thermodynamics using the formula for mixing free energy:

$$\Delta Gmix = \Delta Hmix - T\Delta Smix \quad (1)$$

Where ΔG_{mix} is the mixing free energy, ΔH_{mix} is mixing free enthalpy, T is temperature and ΔS_{mix} is the mixing entropy. This formula describes how various interacting factors play into the mixing of the elements in this composition. ΔH_{mix} being made up of internal energy, pressure, and volume and ΔS_{mix} being Boltzmann's constant times natural logarithm of the number of possible microscopic configurations or microstates of the individual atoms or molecules. These interlinked factors determine how the structure and grain boundaries are formed.

The second sluggish diffusion effect is the factor that involves the phase formations and transformations and how vacancies within the formed structure are filled. Since there are many different elements with slightly different sizes and properties there is room for there to be a slower rate of diffusion within the HEA. This is due to random layering that would occur within unit cells and since all elements are equally likely to occupy this leads to a slower diffusion rate.[5] However, this sluggish diffusion effect is believed to lead to HEA's being able to reach a super saturated state, higher recrystallization temperature, slower grain growth, and higher creep resistance.[8,9] As well as extraordinary high temperature strength and structure stability which could also lead to the formation of nanoprecipitates.

Another effect is from the lattice distortion effect which is due to the variety of different bond energies, atomic sizes, and crystal structure tendencies and these upon occupying lattice sites cause

stress and strains within them.[10] Furthermore, this tends to lead to a distortion in the lattice and since every lattice site could be potentially different from site to site this influences mechanical, thermal and electrical properties both positively and negatively.

The final effect has to do with the mixing of various elements within the structure in turn forming a "cocktail" or mixture of these which have various effects depending on the addition or reduction of an element within the mix. For example, in the past there have been HEAs that have been tested by varying the percentage of one of the elements within the HEA to see how the content change would change the overall structure and properties. One such example comes from studying the microstructure, wear, corrosion, and tribocorrosion behavior of a $CoCr_2FeNiMo_x$ HEA coating onto a steel substrate. These HEA samples were found to have high durability, resistance to creep, and high thermal resistance.[3] This composition included 5 BCC elements with varying properties for each. BCC structured HEA's are known for exhibiting high durability and low plasticity.[11]

There has not been extensive research that has gone into this composition of high entropy alloy in the form of a coating for a thin film. These 5 elements that are used in this target are ones with different desirable properties such as anti-corrosion, high hardness levels, high thermal stability and as well as other properties.[12] For example, Tungsten is the hardest metal there is with chromium in the top 5 hardest metals as well. Furthermore, all the metals demonstrate anti corrosive properties in their elemental form. This mix of element has the potential to exhibit attractive properties as a coating for thin films.

High entropy alloy thin films (HEAF's) as they are sometimes referred to have properties that could have useful applications in different fields.[12] These thin films have shown to have excellent properties such as wear resistance, high hardness levels, high temperature resistance and corrosion resistance.[13] Which could have applied as material for solar energy conversion, thermal barrier

coatings, diffusion barriers as well as others. These mechanical, thermal, and physical properties have led to further exploration into the field.

The application of thin film HEA's leverages the superior properties of nano and micro-structured materials with the known capabilities of HEA's. This leads to thin films with high hardness (in excess of 22 GPA depending on the composition) as well as high crack and delamination resistance. This can be attributed to a variety of factors including the formation of uniform phases in thin films as opposed to bulk HEA's that run the risk of phase separation during formation and a larger grain size based on processing parameters.[11, 13-16]

The structural properties of HEA thin films can be extensively modified via methods such as the introduction of separate metallic dopants such as Ge and In as demonstrated by Braeckman et. Al. The modification of the thin film structure via non-metallic elements like nitrogen and modifying processing parameters such as pressure and temperature also leads to varying properties within the thin films .[17-19] One such example demonstrated by Xia et al. demonstrated that increase in nitrogen content can lead to improvement in hardness values via shift from a body-centered to face centered cubic structure within the thin film at the cost of increased embrittlement.[20] This is a clear indication that more work is needed into understanding the effects of processing parameters of HEA thin films so that the final product can be precisely tailored for a given application

1.1 Motivation and Research Objectives

Based on our groups research into HEA's the have shown there are promising properties that are exhibited such as high temperature stability and excellent toughness.[21] In the past our lab has studied the bulk effects of this particular CrVNbTaW composition in cube form. These cubes were studied intensely by other members of our lab. Moreover, our lab is currently working on the potential of this composition as a catalyst.

Since there are many different properties which HEA's have there are many avenues to be studied in particular its anti-corrosive properties which play a big factor in catalysts. It is important to continue to find new high surface area materials for energy storage as well as materials that are not easily degraded. Therefore, it is important to know the process it takes to fabricate these these novel compositions and at what temperature, pressure, length etc.

CrVNbTaW all have individually exciting properties which therefore spark interest to see how they would interact in a soup like mixing setting. In turn making the refining of these processes is important for the future of material science research. The purpose of the present work is to study the fabrication process, structure, crystallographic information, and mechanical properties.

The specific objectives are as follows:

1) Fabricating the HEA thin films using RF magnetron sputtering on silicon and sapphire.

2) Structural and mechanical evaluation and analysis of samples at different deposition pressures

4) Deposition of HEA using co-deposition of silicon and HEA targets.

5) Structural analysis of the thin film as a function of substrate pressure.

6) Exploring the mechanical properties of HEA thin films.

Chapter 2: Literature Review

HEA's have been broadly ever since they came into the scene around 2004 by Cantor.[22] HEA's have been known for their attractive properties such as excellent hardness, thermal stability and anti-corrosivity.[23] In this particular target Chromium Vanadium Niobium Tantalum and Tungsten were brought together by Plasmaterials through powder metallurgy and in the past this exact alloy has not been published about outside of CMR. There has been however much research into HEA's as a coating since they have been used in such as aerospace materials, catalysts, metallurgical material and materials for nuclear applications[24].

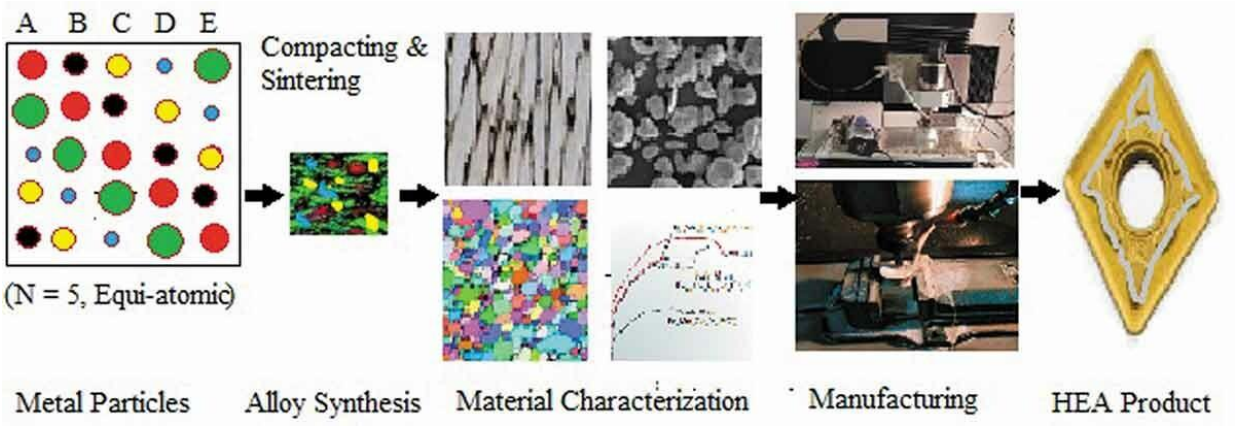

Figure 1.1: Process flow of HEA's [25]

When it comes to high entropy alloys and alloy in general there are many different methods in which they are fabricated and used. The alloying synthesis is an important procedure and there are different methods that can be used in order to have different effects or different properties. For example, there is solid, liquid and gas processing but can include arc melting, induction melting, bridgman solidification, ball milling followed by various powder metallurgy methods or spark plasma sintering sputtering, molecular beam epitaxy, additive manufacturing, thermal spray, laser cladding and electrodepositon.[25] All these different methods to process HEA's involves many different parameters and variables when it comes to each process

Furthermore, HEA's can come in many different shapes and sizes like shown below

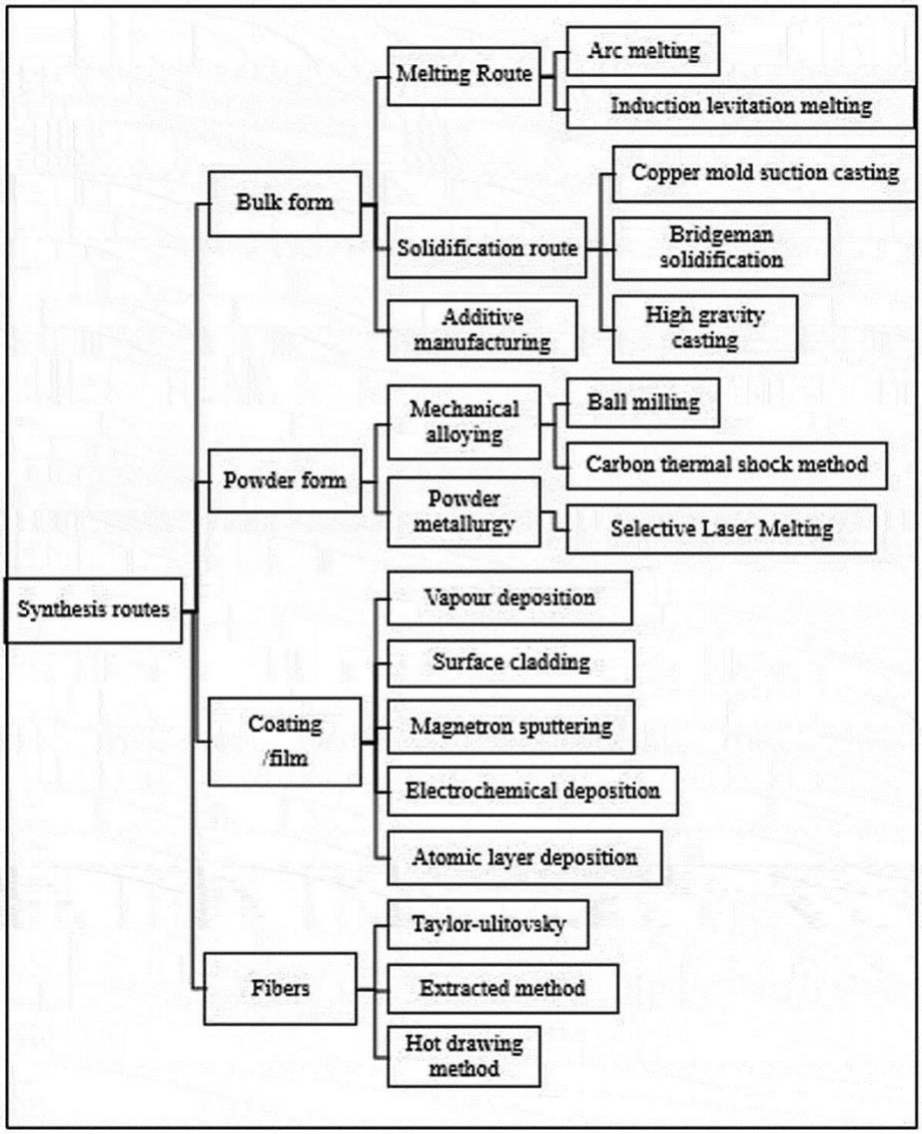

Figure 1.2: Different types of synthesis of HEA's [25]

With all these individual different forms of HEA's there are many different applications for them in their respective bulk, powder, coating/ thin film and fiber forms. Bulk form HEA's ingots are sometimes made to so that these HEA's can be characterized and analyzed. Sun et al created CoCrFeMnNi ingots using a magnetic levitation melting technique to be which found promising properties in terms of strength and uniform elongation.[26] These ingots were found to have attractive

balance of strength and ductility with the Hall-Petch in mind in their fabrication by reduction of particle size through cold rolling and annealing process. This Hall-Petch can be seen as a function of grain size (d) , stress(σ), and material constant through theory or prediction(κ_{HP}).

$$\sigma(d) = \sigma_o + \frac{\kappa_{HP}}{\sqrt{d}} \quad (2)$$

This relationship Li et al found that this effect came from micro-mechanics with availability of an accurate material variable which they go on to explain is useful when interpolated but not so much for extrapolating data.[27] This effect is intuitive since stacking or conglomeration of particles would be easier for smaller in terms of less amount of space between particles.In turn why depositions parameters for HEA fabrications have the need to be optomized. Showing the need for more experimentation to take place in terms of establishing a database for alloys and HEA's in general so there is more usable information for ideal fabrications of new materials and applications of them.

Another form that HEA's may come in is powder. There was a study done on a VNbMoTaW powder which was investigated for its hardness properties. [28] This is important since if Molybdenum was switched for Chromium, we would have the target used in this project. Xin et al found that the smaller the particles in the powder the harder the samples would be since there would be more room for packing and in turn higher particle density. Similar to the ingots above this Hall-Petch relation was explored in this study and found promising results from their formulated powders which concluded that this exceptional hardness may have come from solid solution, grain boundary and dislocation hardening.

HEA fibers can be in a way a bulk form but in a different shape. For example, Li et al formed rods from an AlCoCrFeNi HEA using high-purity elements using vacuum-levitation melting.[29] These rods were essentially elongated cylinders which showed exceptional mechanical properties such

as fracture strength and were able to be stretched out without failure to a high degree. This studied alloy form demonstrated not only the ability to not break when stretched nor when pressed on which can have different useful applications.

Individually each element is fairly similar since they are all transition metals and some have similar characteristics. Below is a table of their overall important properties to give a clearer idea of the parameters that go into the formation that becomes a high entropy alloy.

Table 1.1: Table of Elements within HEA

Element	Density ($kg/m^{3)}$	Crystal structure	Melting point (°C)	Radius (picometers)	Hardness(MPa)	Weight (amu)
Chromium	7190 kg/m^3	BCC	1907	166pm	1120	51.996
Vanadium	6110 kg/m^3	BCC	1910	171pm	628	50.94
Niobium	8750 kg/m^3	FCC	2477	198pm	736	92.906
Tantalum	16,650 kg/m^3	BCC	3017	200pm	800	180.95
Tungsten	19,250 kg/m^3	BCC	3442	193pm	2750	183.84

Silicon	2,330 kg/m^3	Diamond cubic	1414	111pm	1130	28.085

From these different properties we can see how certain elements may act during the deposition process. For example all are body centered cubic crystal structure except for niobium and silicon which can lead a different or awkward packing when the alloy is brought together. Another could be the large jump in density in tantalum and tungsten and therefore these heavier atoms could form and dislocate other atoms differently from the others. Overall all show fairly hard levels that are attractive for the purpose if this experiment.

These differences play a role in how effective or purposeful a coating can be. For example, Chromium in an HEA study was found to have shown increasing hardness properties as Chromium content in the HEA increased.[30] Chromium being known for being one of the hardest metals as well as being used to harden steel. There are other uses for Chromium and its various properties and uses can also including plating and reflective coatings.

Chromium is one of the main elements in the making of stainless steel due to its attractive anti-corrosive properties. Chromium's ability to form a passive oxide layer and the less dissolution of a surface the less corrosion that occurs. In a study on surface corrosion Ma et al found that the addition of chromium to an iron alloy helped with the dissolution and diffusion of a surface based on a formula to do with thickness measurements.[31]

$$R = \frac{a-b}{2t} \quad (2)$$

where, R is the corrosion rate (mm·h^{-1}), a is the original thickness (mm), b is the final thickness (mm), and t is corrosion time (h). It showed that with chromium addition surface degradation was decreased to a degree.

Vanadium is another element present in this HEA and is similar to Chromium in size, density, melting point as well as others since they are both present in the 4^{th} period of elements. Vanadium is an element that is also known for having excellent hardness values and is also used in the making of steels. Another study that demonstrated the behavior of vanadium in an HEA was one done by Dong et al which found high levels of compressive strength and plastic strains as well as Vickers hardness.[32] Another similar study found similar results in terms of increasing hardness with increasing vanadium content but also showed excellent wear resistance also.[32]

The only 5^{th} period metal niobium is another element in this particular HEA composition that also has attractive properties like chromium and vanadium. This particular study found the increase of Niobium content in a $TiHfZrNb_x$ high-entropy alloy was correlated with an increase in corrosion resistance. [34] Specifically, through a series of static and dynamic electrochemical tests and surface characterization testing for niobium's role in passivation and dissolution.

Similar to vanadium a study found that the addition of niobium to a AlCoCrFeNi HEA correlated to an increase in the compressive yield strength and plastic strain measured.[35] This similarity between vanadium and niobium is understandable considering their respective placements on the periodic table. Which in turn allows for certain different phases to be formed within the context of this particular HEA and interestingly much work has gone into discovering new phases and new materials. Atomic size differences (δ), electronegativity (χ), thermodynamic parameters (ΔH_{mix} and Ω), and valence electron concentration (VEC) are theorized to play an important part in phase formation but still much research into the subject remains.[36]

Tantalum one of the two elements in the 6^{th} period is one that is known for its properties similar to its other members of this HEA which include low ductile-to-brittle transition temperature, high ductility, good workability, good corrosion resistance to liquid metals and high strength at high

temperatures.[37] From this study it was found that these films fabricated showed decreases in surface roughness since an increase surface roughness can lead to electrical shorts this was an admirable property found.

The final and largest element in the HEA is Tungsten which is hardest of all and has similar traits to the others but different ones as well. In one extensive study not only were promising hardness values found but also corrosion similar to previous members of the HEA however these were a to a certain degree higher.[38] Out of all the elements present within this HEA composition tungsten's properties might be the most impressive for various reasons. One study went so far as to categorize them as their own type of HEA being TCHEA's (Tungsten containing HEA's). [39] This study found that not only were TCHEA's hard and resistant to corrosion they had potential for being plasma-facing materials in the fusion reactors. This is due to their irradiation resistance, toughness and high melting temperature.

All together these elements all can complement as well as hinder one another when it comes to them being brought together to form a coating for a thin film. In reality since HEA's are still in their infancy so to speak there is still lots of room for growth and since methods to optimize their fabrication work still needs to be done. Ye et al explain that there is not yet a general and expansive theoretical model for the prediction of the formation enthalpy of an ordered compound HEA.[40] In general entropy within alloys is a study that has gain attraction for research but has not yet been improved drastically.

Zhang in his study used calculation of phase diagrams (CALPHAD) in order to get an idea of the thermodynamic inter play between elements when forming into compositions through computational methods.[41] In order to see how the formation was like, databases and previous experiments were used to drawn upon to establish a simulation of phases. Using various different

parameters and variables to create systems of that contain amounts elements and diagrams give us an idea of what is made. With that being said there has not yet been a CALPHAD study done on this particular composition.

In terms of HEA thin films much research over the years have gone into finding new combinations of HEA's and constantly bettering the different properties. One such example is NbMoTaW high entropy alloy thin films which showed very promising electrical and mechanical properties[42]. According to Feng et al these films showed superior levels of hardness as well as demonstrating strong size-independent electrical resistance. They were also made using DC instead of RF magnetron sputtering however these results proved promising since this alloy included 3 out of the 5 elements used in our samples.

Xiao et al found similar results to Feng in terms of high strength and enhanced fracture toughness. Which was found through micro cantilever bending and deposited using ion beam assisted deposition.[43] Moreover, there was a fairly similar study done on CrNbTaTiW-C HEA thin films which spoke about the elemental distribution of it and how carbons addition played a role when added to the alloy.[44] There are many different studies being done on this topic of research so it is important to add to the library of knowledge on the material science of alloys and their uses.

Chapter 3: Experimental

3.1 Sample Preparation

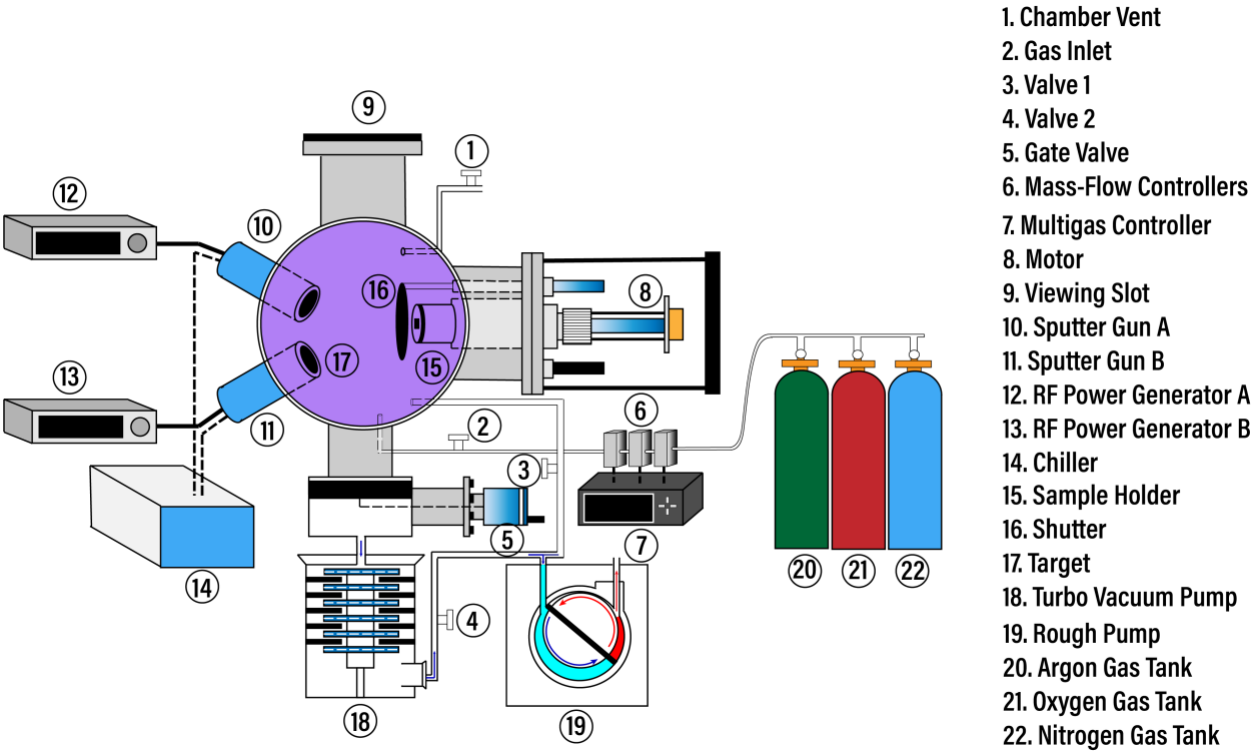

Figure 3.1: CMR's sputtering system diagram

RF-sputtering was used to deposit nanocrystalline CrVNbTaW coatings onto silicon (Si) (100) and Sapphire wafers. Before the depositions substrates were ultrasonically cleaned and sonicated using the Bransonic CPXH ultrasonic bath. Any excess solution on the wafers was dried using an Imp Air-Blower and Kimtech Task Wipers before being introduced to the deposition chamber. Using a roughing pump (Edwards E2M30 Rotary Vane Pump) and turbo pump (Pfeiffer HiPace 80 Turbo Pump) an operating pressure of ~10-6 Torr was reached. A CrVNbTaW target (Plasmaterials, Inc.), of 2 in. diameter and 99.999% purity, was utilized and a 2 in. sputter gun located 7 cm at a 25° from the substrate. The sputtering voltage of the Cesar RF Power Generator Power was gradually increased to target until 100 W was reached. High purity argon (Ar) gas was introduced into the chamber via MKS mass flow meters at a rate optimized for the sputtering chamber of 40

sccm. Pre-sputtering was done on the target for 15 – 20 min with a closed shutter above the gun. Once the shutter was opened and desirable substrate temperature (600°C) was reached the deposition was done for 1 hour for each sample. A PolyScience chilling unit was utilized throughout the deposition to prevent over-heating of the electron guns. The samples were rotated during the entire deposition to ensure consistent coverage of the whole surface of the substrate. The samples were then allowed to cool to ~25°C before removal from chamber.

For the 1st set of fabricated samples there were 2 substrates being coated at the same time one being silicon and the other sapphire. They were done for 1 hour, at 600C, with 100W of power to the HEA target in the gun with the previously explained procedure 10 samples at varying pressures during depositions of 0.1, 0.5 , 1 , 1.5 and 2 mTorr in total producing 10 samples.

The 2nd set was done with a different the same constants as the 1st but there was an effort to try and incorporate silicon onto the same target using silver paste to attach them onto the target during deposition 3 attempts were made but, on the 3rd, attempt the target began to spark and degrade rapidly which led to another route. Which involved a change of a substate and a new target.

For the 3rd set of samples were done with a different idea in mind this time. Using a new substrate in this case being steel (insert details) came in sheets. These were made into square to fit the substrate holder in the sputtering chamber utilizing the Mechanical engineering machine shop. The steel substates were then deposited on using a similar procedure as the sapphire and silicon ones. 5 samples were fabricated at varying deposition pressures same as the ones listed above using identical procedure.

The last set was done by incorporating the use of a 2nd target which was a plasmaterials Si target (insert details). This target was used on the other gun and varying watts of power were supplied to the during at the beginning of the deposition. Same parameters as above except the same pressure

was used for the different samples with varying power supplied to the Si target. However, this time the co-depositions were done onto FA140521 Stainless Steel - AISI 304L substrates. Which were studied to study how the effect and intermixing of substrate and coating was different from sapphire and silicon.

3.2 Radio Frequency Magnetron Sputtering

The samples were fabricated using a RF Magnetron Sputtering system. This is a physical vapor deposition technique. Which uses a chamber in a vacuum environment with an electrical field in it as well as an inert gas to be able to knock off particles from the target onto the substrate.

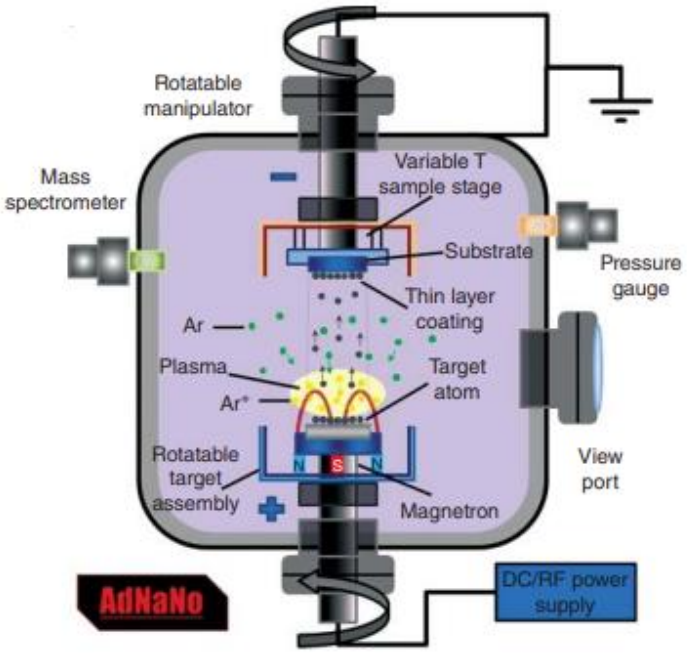

Figure 3.2: Magnetron sputtering working principle [45]

The material that is sputtered off of the target travels from the plasma cloud and nucleates onto the surface of the substrate. Inert gases are used since they aid with the sputtering to knock of material from target and its solidifying on the surface. The term sputtering comes from the phenomenon in which microscopic particles of a solid material are ejected from its surface, after the material is itself bombarded by energetic particles of a plasma or gas[46]. Since these particles from the inert gases do not form bonds with the elements inside the chamber these gases able to aid with deposition and sputtering process.

Table 3.1:List of samples made

Gun used on substrate	**Substrate Temperature**	**Power to gun, Operating pressure**
HEA on Si and Sapphire	600°C	100W,0.01 mTorr
HEA on Si and Sapphire	600°C	100W/0.5 mTorr
HEA on Si and Sapphire	600°C	100W/ 1 mTorr
HEA on Si and Sapphire	600°C	100W/ 10 mTorr
HEA on Si and Sapphire	600°C	100W/ 20 mTorr
HEA and Si on Steel	600°C	100W/0.01,0.5,1,10,20 mTorr

HEA and Si on Steel	600°C	20,40,60,80,100W for Si/100w for HEA ,0.1mTorr

These samples that were made in this case were made in this set up which was an Excel instruments DCSS-12 RF magnetron sputtering system, an Edwards E2M30 Rotary Vane roughing pump and Pfeiffer HiPace 80 Turbo Pump and Cesar RF Power Generator Power.

3.3 X-ray Diffraction (XRD)

In terms of characterization of materials XRD is one of the most used tools for analyzing a myriad of different liquids and/or solids. This technique is not just used by material scientists but many other different fields as well. Madam Curie who was known for her discovery of radioactivity through the use of x-rays for diagnosis and treatment of soldiers in World War I. [45]Thanks to her discovery now we are able to know more about the crystal structure, identifying phases and symmetry. The working principle behind XRD lies in Braggs law which has to do with the difference between incident and diffracted waves and based on that mathematical relationship we are able to say something about the atomic planes.

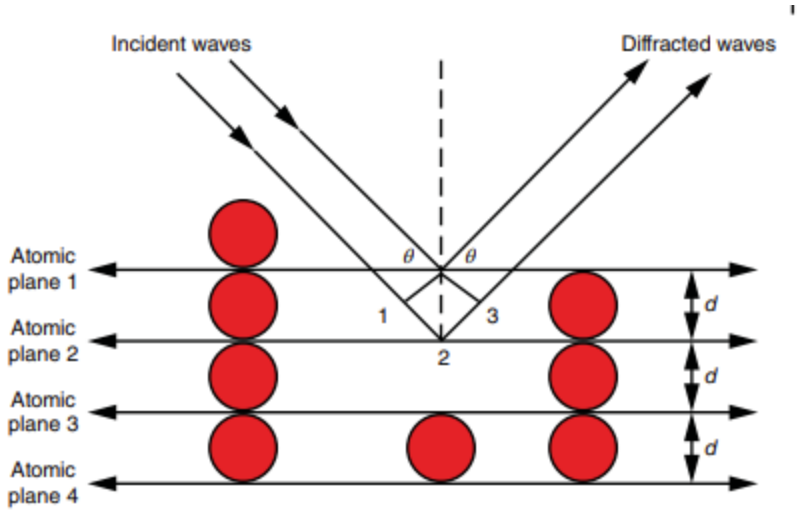

Figure 3.3: Visualization of X-rays and Braggs law [45]

Essentially a single-color beam discharged from a source which are shot at a surface at certain angles and bounce back generating certain peaks at certain angles. Which can therefore give us an idea of the sort of structure which is present on the surface. In our case since we are characterizing thin films, we need to use GIXRD to be able to avoid substrate interference. A Malvern Panalytical Empyrean Nano edition multipurpose X-ray diffractometer was used in Bragg–Brentano reflection geometry. To resolve each peak from the diffraction pattern clearly, θ/2θ scans with a step size of ° and an integration time of s/step were conducted on the thin films at room temperature. A Cu Kα X-ray source with a wavelength (λ) = 1.54 Å which was used to obtain the values. The substrate peaks were some of the biggest peaks which were discarded to accentuate the gathered data. Xpert highscore was used to try and identify the peaks since there was very little data on alloys let alone HEA's there were many peaks that were left unidentified.

In terms of peak identification there has not been too much research that has gone into developing a backing of scans taken for XRD's. however there have been many studies which have undergone much research when it comes to peak identification in HEA's. In defining peaks binary and tertiary systems are very important because without them there would be no data to draw upon from.

However even these in themselves happen to be fairly limited so there grows a need for a more extensive backlog of data for XRD scans for HEA's. Which is why studies like these are important to pursue so that in the future HEA structures can be more easily identified.

3.4 Atomic force microscope (AFM)

In this particular piece of equipment Hooke's law is used to study the surface of samples using a specialized tip that based on the relationship with force applied on a cantilever and deflection and stiffness when the force is applied to it. Depending on the distance from the sample to the cantilever there is a laser that measures that distance. Using a photodiode which picks up on those photons from the laser and is able to send it to a detector. These images are produced based on the effect of either Columbic or van der Waals forces causing a probe to deflect and measured using a piezoelectric transducer.

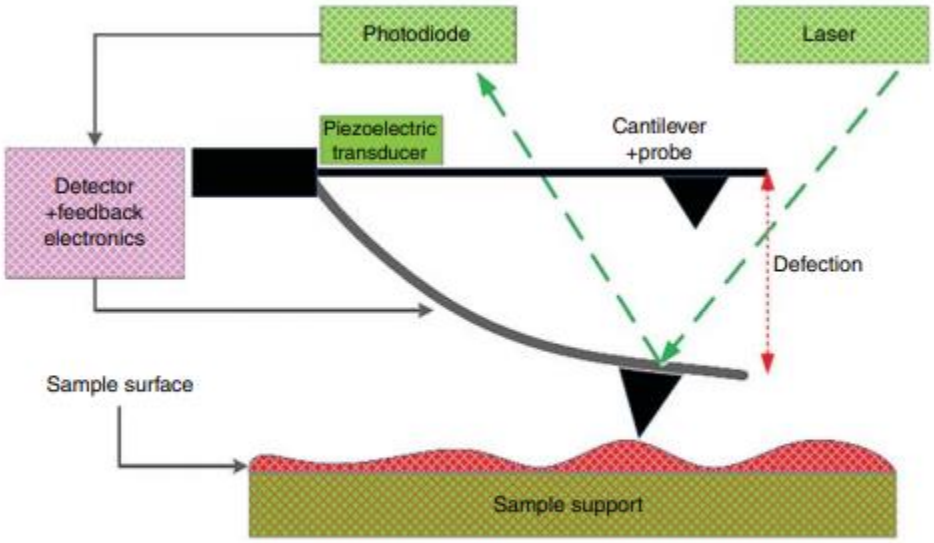

Figure 3.4: AFM probe working principle [45]

In this case studying the surface morphology of each sample is important to get an idea of the structure and to try and get an idea of the grains and their sizes as well as get idea of peaks and

valleys on the surface. The thin film samples were characterized using a Nanosurf Naio AFM in phase contrast mode with CCSR-10 conical tip was utilized in the instrument where the 1 × 1 μm scans are acquired with 356 points/line and a time per line of 4 s for a total scan time of around 25 minutes each. Using WSXM and Gwyddion software these images were smoothed and flattened to generate the images we have now. All samples' images were obtained with the same procedures and processed with the same software for all of the films.

3.5 Nano/Microindentor

For hardness analysis of these samples there were 2 different pieces of equipment which are a nano and microindentator. Firstly, the nanoindentor which used was a Hysitron T1750 Tribo nanoindentor with an attached triangular pyramid Berkovich diamond indenter with a normal angle of 65.3° between the tip axis and triangular pyramid faces was used for the nanoindentation. The effective size of the apex was approximately 100 nm and the indents were done on with increasing force (mirconewtons) until the predicted 10% indentation depth was reached and then the 25 indents were done at that force to calculate hardness and other values. For this it is important to have an idea of what the approximate thickness of the coating is in order to obtain accurate results. The working principle behind indentors has to do with Pharr and his method of using a formula involving the elastic modulus, stiffness and area as well as using the relationship between hardness and maximum load over area. The method developed by Oliver and Pharr was employed to calculate the mechanical characteristics (H and Er)[47]. Using this method, Er can be calculated by finding the stiffness (S) of the film from the slope of the unloading curve. The relation between Er and S can be described using:

$$E_r = \frac{\sqrt{\pi}}{2}\frac{S}{\sqrt{A}} \tag{3}$$

where A is defined as the area of contact at peak load. To find the hardness values, the same value for area of contact is used along with the maximum load (Pmax) in:

$$H = \frac{P_{max}}{A} \quad (4)$$

When nanoindentation yielded results inconsistent with the theoretical expectations, supplementary measurements were done using microindentation. (Struers Duramin-A300) Hardness and modulus values were calculated as above. These formulas combined can give us an accurate idea of the young's modulus of elasticity as well as the hardness level for the sample. These penetration depths and depending on how deep and easily the tip is unloaded will usually determine how hard a sample is and also how elastic the surface is if it can deform plastically or permanently.

For the samples that were evaluated with the Hysterion there were only a few that were able to be analyzed accurately since the equipment had to be fixed twice. Even though a lot of data was obtained from this system a large portion of it had to be discarded due to an error in the reading having to do with the stage and the outputted readings. The results that were able to be used were shown later on.

Following the 2nd break down of the Hysterion another option was needed to be explored which involved using a Streurs Duramin A-300 to determine the surface hardness of the samples surface. The procedure for this piece of equipment is the same as nanoindentor but it is done at a micro scale and has higher force and is less precise in terms of its measurements. It must be noted that it was found that for the steel samples compared to the sapphire and silicon samples the values were drastically different even though they were deposited in the exact same conditions.

3.6 SEM/EDS

Scanning electron microscopes create images through the detection of backscattered electrons. They tend to be used to see images of a surface using dispersive x-rays which hits away an atomic electron from its shell leaving a hole which is filled by another electron that gives off a distinctive x-ray. These rays are detected in order to give us an idea of the material that is present depending on the energy level the x-rays spike at. For example, there are certain elements that have distinct peaks on the x-ray energy spectrum.

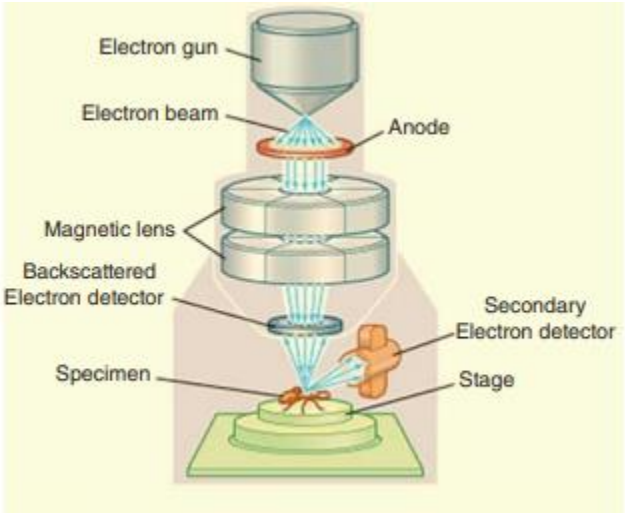

Figure 3.5: SEM working principle [45]

These particular samples were evaluated in using similar methods for each. Each sample was imaged first with the SEM and using that image and frame size the EDS scan was taken with same length and settings for each sample. With each scan a new spectrum was found which was the bases for establishing molecular weight percentage ratios. It was possible to get an idea of the percentage compositions of a certain image depending on the elements present from that said frame area.

In this case the scanning electron microscopy was performed on the surface of the thin films with a Hitachi SU 3500 using the backscattered electron and secondary electron mode. The relative

elemental composition was determined by EDS with the use of x-ray color mapping to allow for the determination of dispersion of individual elements.

Chapter 4: Results and Discussion

4.1 X-ray Diffraction (XRD)

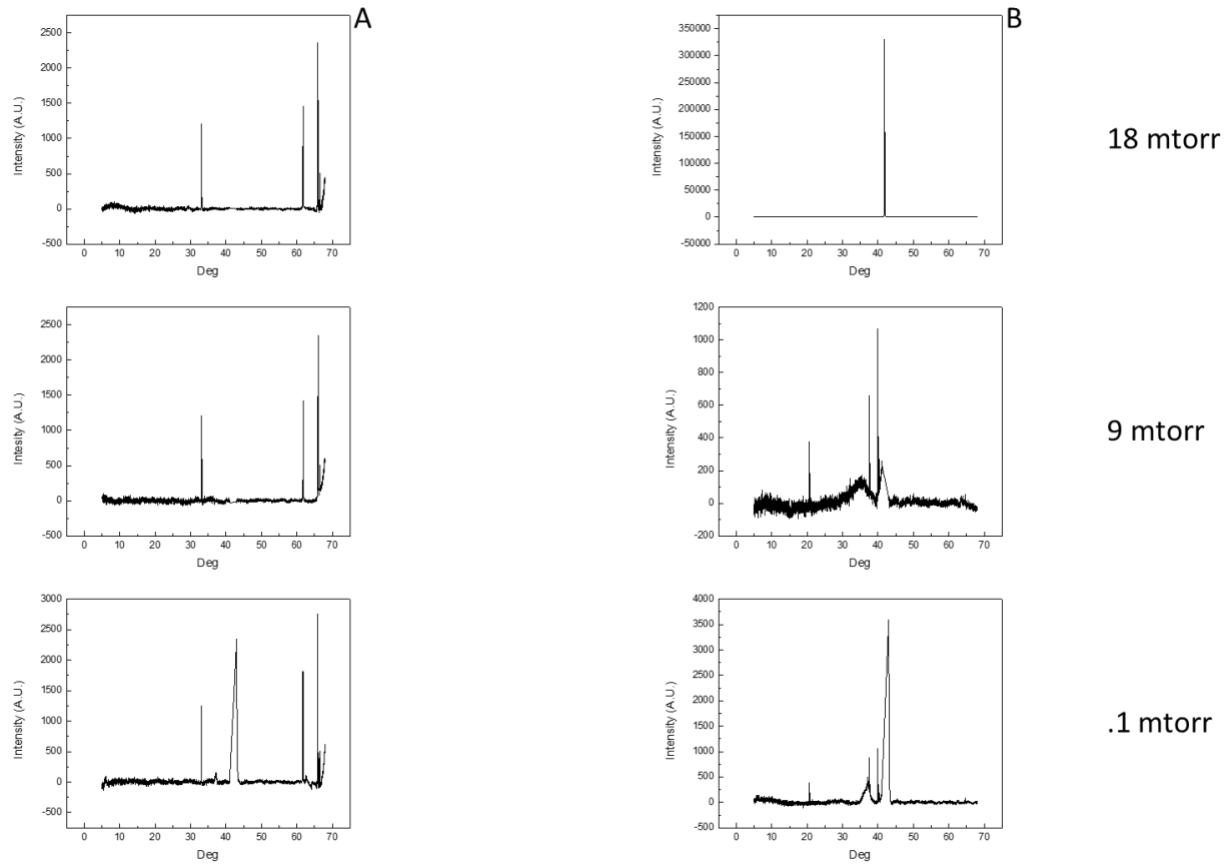

Figure 4.1: A)XRD data for Si substrates, B) XRD data for Sapphire substrates

The HEA thin films, while deposited under varying pressure, were all kept at the same elevated temperature, leading to a relatively stable and consistent chemical makeup for the coatings as indicated in figure 1. The exception to this seems to be at the elevated pressure where there is a high potential for atomic scattering of the lighter elements and resulting in a slightly skewed elemental makeup for the films in question. There is also variability associated with the substrate

in question as indicated both by the varying peak patterns present between silicon and sapphire substrates, and the fact that at the highest-pressure deposition, only a single substrate peak is measured for sapphire.

Like was mentioned in previously there was no exact XRD scan done on this sort of sample before. Due to its novelty the exact identification of peaks posed to be a challenge. Using Xpert Highscore the peaks were in a way inferred using this software based on past XRD scans from a large database. These databases contain a myriad of different compounds that have been test using XRD and have their results published so that they can be compared. From these results the substrate peaks were removed and it showed that at 36 and 44 degrees non substrate peaks appeared.

These 2 peaks occurred on both the sapphire and silicon substrates and from what was found on xpert highscore from a peak identification search using an extensive database the peaks were able to be guessed. At 36° there is a small broad undefined peak that is gradually increasing in the silicon samples. Although this peak was not defined as intense enough to be considered one for the sapphire samples, we can see a much more intense peak occurring at the same spot. Xpert gave indications that this peak show a (110) chromium peak position. This could be for a number of different factors including substrate interference or the favoring of mixing with sapphire rather than with the silicon substrates. However, since this is novel work there is not way to be certain only to make conclusions based on information that is available.

The peak at 44° showed strong indications sharing a peak with (110) SiCr although that was the only matched peak congruent with the binary compound SiCr. This could be indicative of an inter layer mixture between the silicon substrate that formed and since silicon has shown favorable properties in terms of combining with HEA’s as well as other alloys. In order from the highest

deposition pressure to lowest we can see the sharpening of the peak and its intensity increase as pressure decreases.

Although for the sapphire substrates the peak is very small but we can see its presence nevertheless. This goes along with predictions that the better the vacuum in the chamber during deposition the better the thin film developed. The vacuum facilitated the deposition and made it easier sputtering to occur which led to increased deposition rates which in turn can lead to thicker coatings.

There is no full proof way to say with 100% certainty what exactly a peak is since the system is just using past examples to come up with a matching peak at that location. However, there are many different compounds that may have a peak at that location or may they may have shifted slightly. This goes back to the binary and tertiary systems of the different elemental combinations that can occur between chromium, vanadium, niobium, tantalum and tungsten as well as the intermixing of layers between substrate and forming HEA layer during deposition. Since there was no past scan of an HEA like this one and as was explained previously outside of our laboratory.

4.2 Atomic force microscopy (AFM)

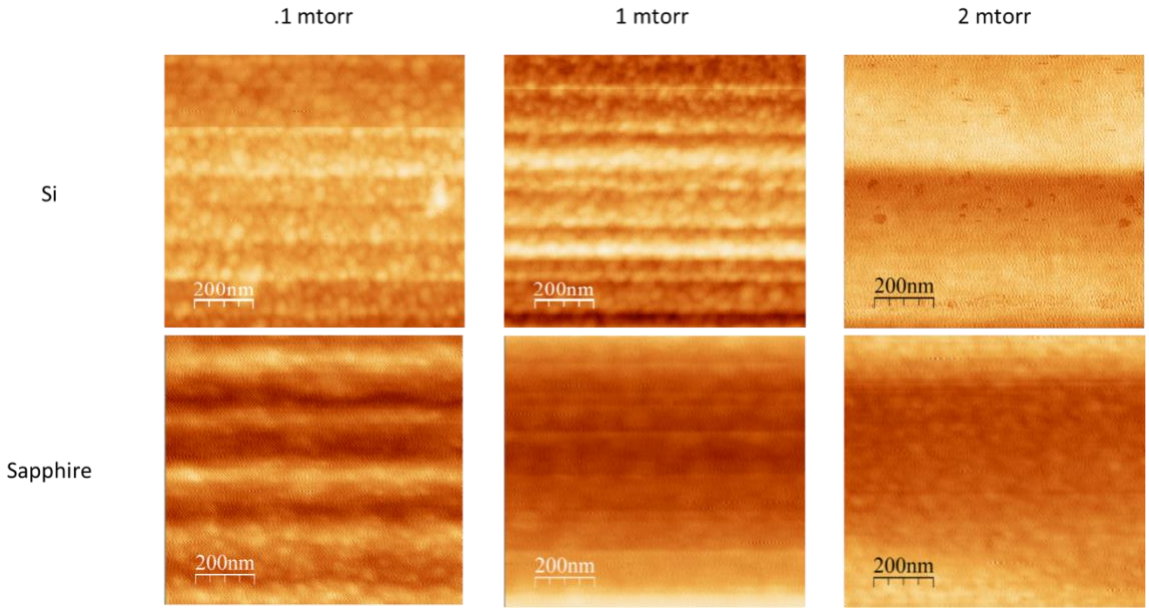

Figure (4.2): Silicon and Sapphire substrate afm scans at .1, 1, and 2 mTorr

The atomic force microscopy scans shown in figure 2 indicating deposition at the lowest, highest and intermediary pressures show a discernible trend in grain size formation with the largest grains and most uniform grain formation apparent at the lowest pressure deposition. While normally an increase in grain size would be associated with a change in the internal energy of the grain structure brought about by temperature change, this is clearly not the case here as all the depositions were carried out at the same temperature and no post deposition annealing took place. Instead, the most likely mechanism seems to be a coalescence of an increased number of constituent atoms within the individual grains at lower pressure. This is supported by the more uniform elemental compositions at lower pressures indicated in the XRD measurements, as well as the consistent and overlapping chemical signatures indicated by the EDS measurements as discussed below.

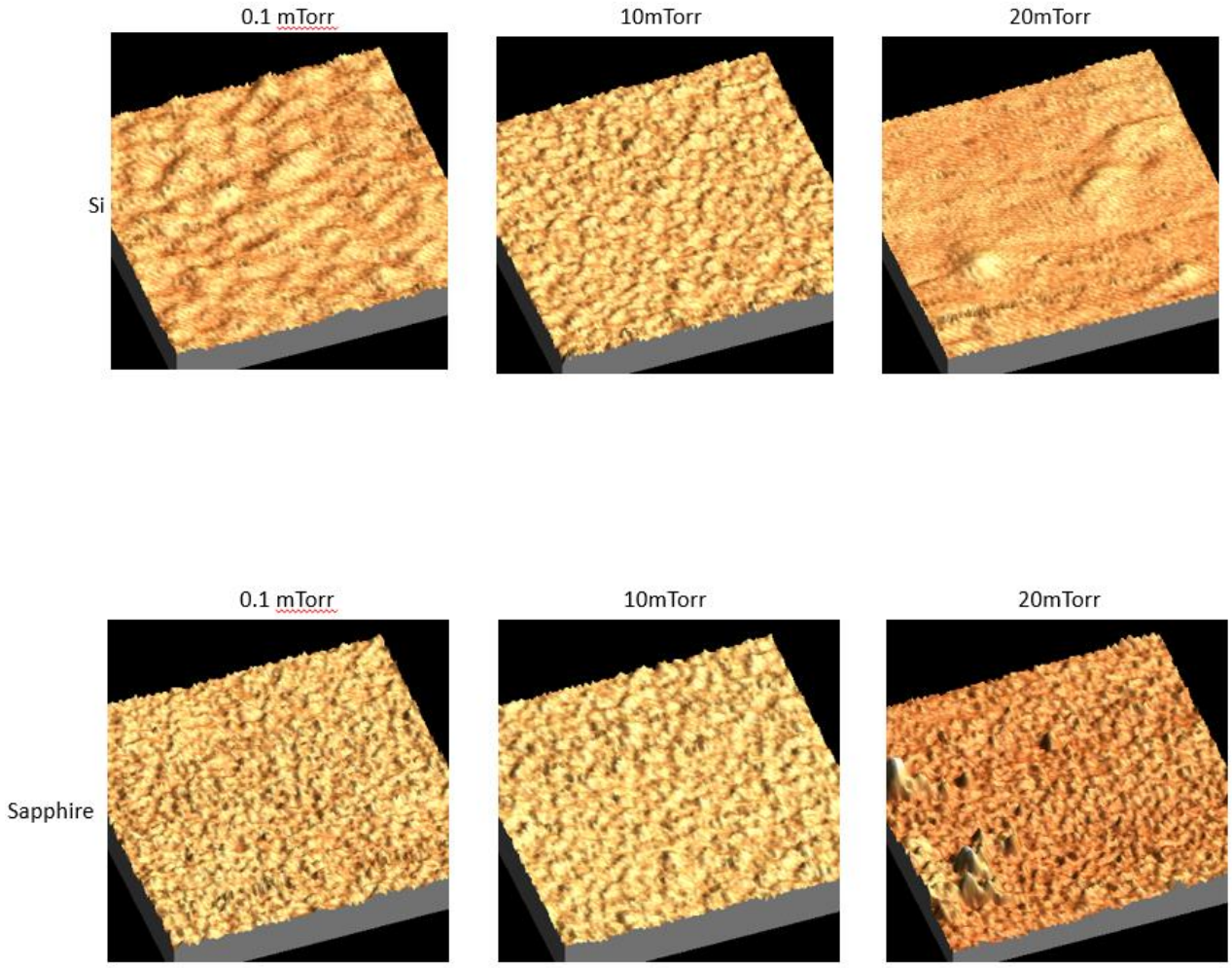

Figure 4.3: 3D images of Si/Sapphire samples of 0.1, 10, 20 mTorr

Like was mentioned previously as deposition pressures were lowered there was a gradual increase in the deposition rates which showed in the largest and uniform grains from the AFM scans. Overall, there was a search for the correct parameters to be used for this experiment. Since there was finer grain formation or more so something like more molecules being able to be packed into a space. AFM scans showed these fine grains more easily distinguishable in the lower pressure samples and was confirmed when the lowest pressure showed clear images of distinguishable grains.

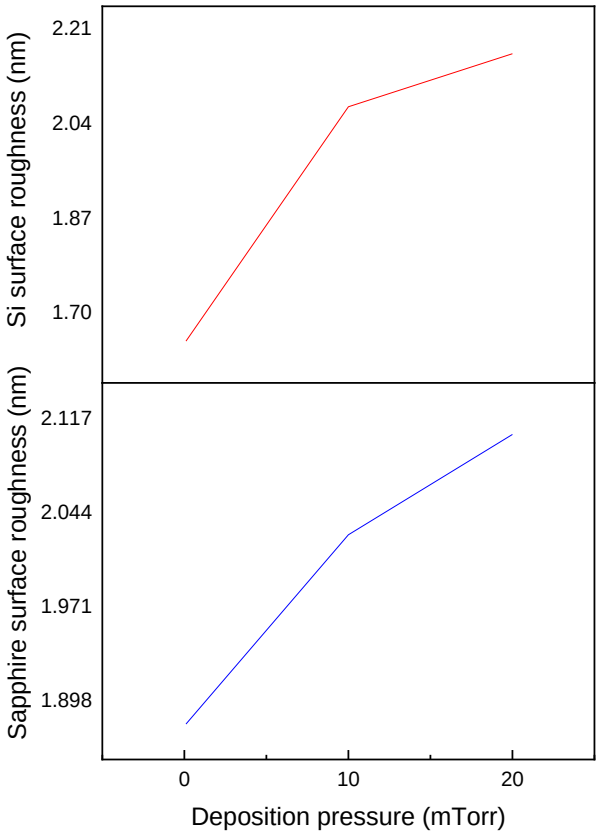

Figure 4.4: Surface roughness data for Si/ Sapphire samples

Another observation that was made in terms of variance from sample to sample was the decrease in surface roughness as deposition pressures began to decrease which was corroborated with the figure above. Although there was not a clean-cut way to determine the grain size of each sample since there was a generally flat and featureless. Could be due to amorphousness in the earlier samples and as depositions parameters were optimized there was a greater degree of crystallinity which was shown in the sharper more intense peaks that were seen in the lower deposition pressure samples. We also see all together the forming of new peaks in samples which could be due to the changing of phases and increasing crystallinity.

4.3 Energy Dispersive Microscopy/ Scanning Electron Microscopy (EDS/SEM)

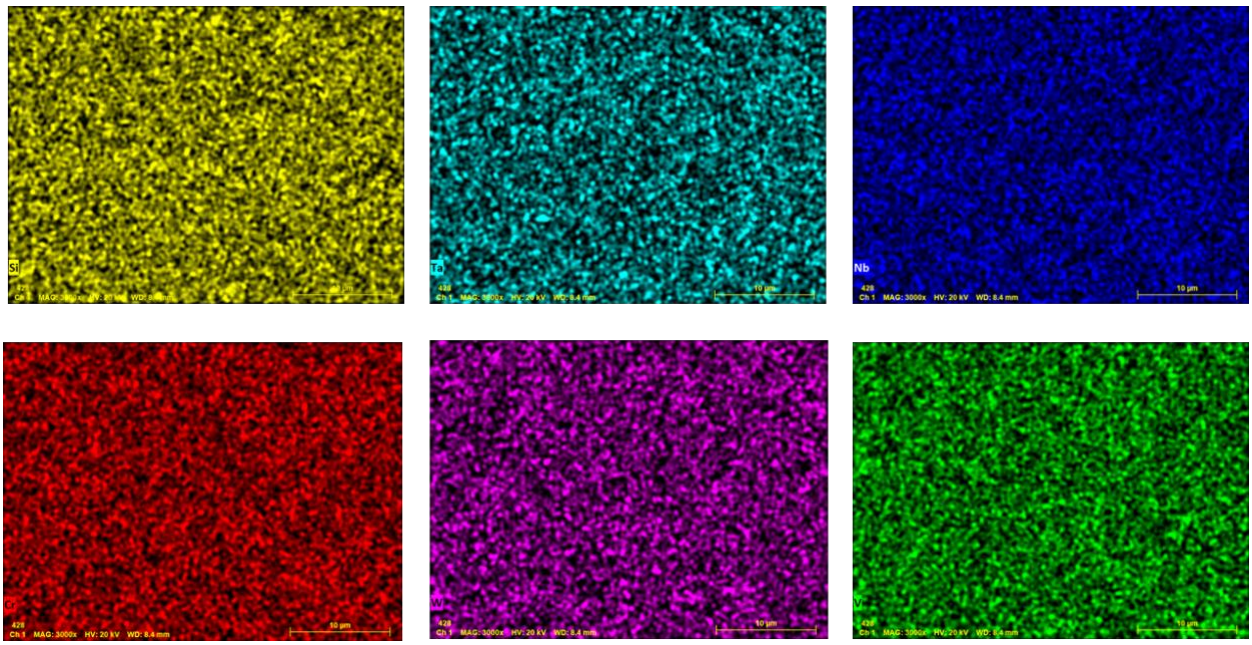

Figure 4.5: EDS imagery of HEA thin film on Si substrate. From top left elements are Si, Ta, Nb, Cr, W, V

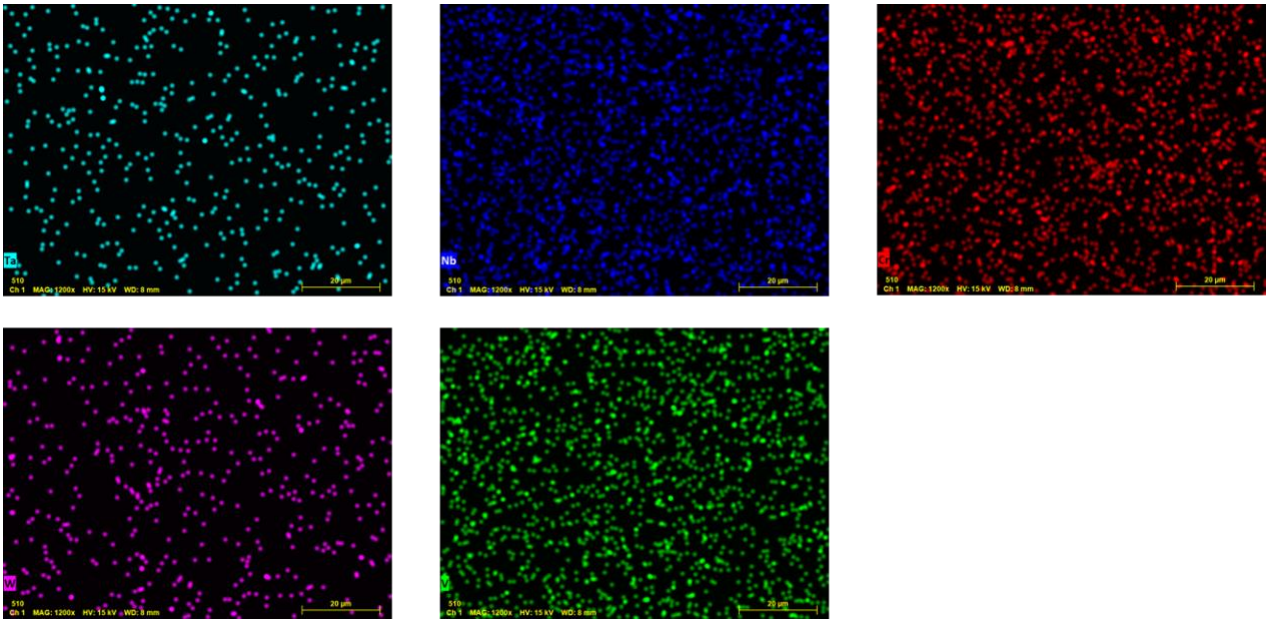

Figure 4.6: EDS imagery of HEA thin films on Sapphire substrate. From top left elements are Ta, Nb, Cr, W, V

EDS measurements were performed on the HEA sample deposited under the lowest pressure to minimize the influence of elemental scattering indicated in earlier XRD measurements. The results, presented in figure 3, seem to support the conclusion derived from XRD as elemental distribution is fairly uniform without an excessive concentration of the heavier elements such as tungsten that can be expected at the higher deposition pressures. The one unexpected result demonstrated in the EDS imagery is a level of Si that is similarly uniform within the coating. This may be attributed to the combination of the high temperature of the substrate, as well as the high energy plasma destabilizing the surface layer of the Si substrate, and the relatively thin film (<1 micron) allowing for relatively even incorporation and diffusion of the Si atoms throughout the film. Figure 4 however indicates potential secondary issues with adhesion has concentrations of tungsten and tantalum are lower than the remaining constituent elements despite deposition at the lower pressures. This adhesion issue is supported by earlier xrd measurements indicating reduced adhesion of certain elements on sapphire as opposed to silicon.

Table 4.1: Elemental percentages found from EDS data

Silicon samples	Cr %	Va%	Ni%	Ta%	W%
0.1 mTorr	15.35%	13.22%	16.43%	26.48%	28.51%
1 mTorr	17.17%	12.24%	32.29%	15.39%	22.91%
2mTorr	19.95%	15.02%	23.11%	13.01%	28.89%

Sapphire samples	Cr %	Va%	Ni%	Ta%	W%
0.1 mTorr	13.89%	10.81%	28.71%	17.94%	29.20%
1 mTorr	11.81%	8.65%	21.87%	21.12%	36.55%
2mTorr	13.52%	8.72%	28.31%	15.8%	33.65%

These tables shown above show the elemental quantifications that were found from the EDS data obtained. Although there is no noticeable trend from the percentages found there was a high percentage of Tungsten present within the samples which could be due to its high density and bonding abilities. From these obtained data collections there was slight indication of lower percentages of lighter elements at higher deposition pressures and gradual increase in heavier elements in lower deposition pressures. Nevertheless, since there is a high order of disorder in these type of HEA samples there is difficulty with the exact calculations of the elemental percentages. For all sampled that were analyzed all had something within 25-30% of relative error percentage.

4.4 Mechanical Properties

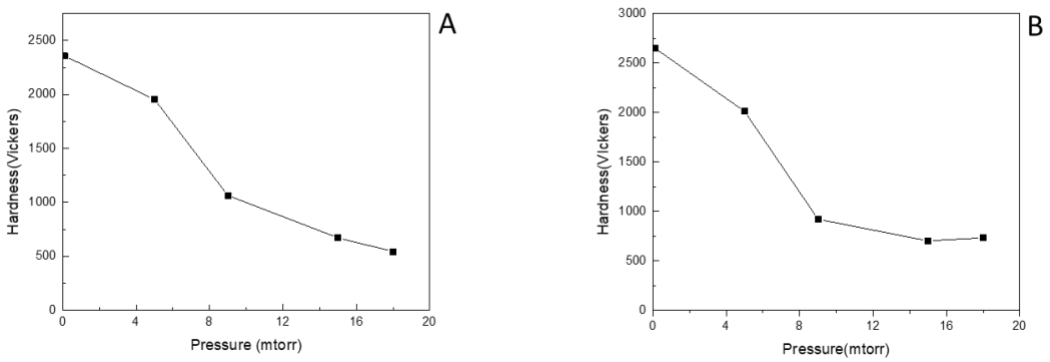

Figure 4.7: A) microindentation hardness values for Si samples, B) microindentation hardness values for Sapphire samples

Figure 4.7 shows a clear trend in increasing hardness values with decreasing deposition pressures. This can be largely attributed to a reduction in atomic scattering enroute to the substrate leading to denser formation of the HEA on the substrate. These results also correlate with the EDS measurements that show a relatively uniform deposition across the samples, indicating minimal phase separation and hardness values that remain consistent across the entire surface of the thin film. The somewhat sharper decline in hardness present in the sapphire samples can be attributed to the pattern of reduced element adhesion compared to silicon, though at the highest pressures the difference is negligible. This also explains the slight increase in hardness at the highest pressure reading as xrd measurements indicate minimal, if any, actual deposition, leading to the conclusion that the hardness value measured is heavily skewed by substrate effects. The microindentor data indicates that even small variances in processing parameters, in this case deposition pressure, can yields significant changes to the mechanical properties of an HEA thin film.

Figure 4.8 Sapphire, Silicon, Steel micro indentations

These above images were obtained from the micro hardness tester and starting from the left to right are sapphire, silicon and steel HEA coated sample. Since all used the matching parameters including same tip and same indentation force as well. We can see with the micro indentor that there may be some sort of substrate effect from the insertion of the tip. Since Sapphire tends to have higher levels of hardness than steel and silicon there was a difference in the shape of the indentation and was also seen in the hardness level that were measured from the samples. However, in the microhardness testing for the steel samples there were low levels of hardness that were being found. This could be due to substrate effect coming into play and instead of the coating being penetrated through it is just crushing the substrate and causing the hardness level of steel to be measured instead. Which was verified when a sample of undeposited steel was measured for hardness and found similar level to those of the steel samples but significantly lower than the silicon and sapphire.

The hardness levels for the undeposited substrates in themselves are fairly hard on their own and with the addition of these coatings we saw an increase in the obtained hardness levels as deposition parameters were optimized.

Chapter 5: Conclusion and Future Work

5.1 Conclusion

RF magnetron sputtering was successfully utilized to deposit a CrVNbTaW high entropy alloy thin films onto various substrates. Subsequent characterization of samples, which were deposited under varying pressures and at a constant elevated temperature, via XRD, EDS, AFM and microindentation, has indicated a significant variance in the mechanical performance of the thin films while maintaining a consistent chemical state and a uniform elemental phase distribution.

Although these samples were not idealized and optomized to the level that was expected. This was due to the main instument of the study the nanoindentor being down for the whole of the study. The entire orientation of the study shifted from hardness, toughenss and elastic modulus study to a corrosive and general study. Despite many tests being left out there was still substatial data published produced when it comes to surface hardness, topography, anti-corrosiveness, and elemental composition. Which could in the future help with the development of new alloys or HEA devices.

In particular this CrVNbTaW HEA has many different attractive characteristics that researchers and engineers could begin and continue to have use for. With the addition of silicon into this compostion it adds a different dynamic to the coating that is formed. Silicon being one of the most abundant elemtns on the planet it is important to have it play a part in the world sustainability and search for new materials and applications.

5.2 Future Work

The next stages of project would involve deposition of the HEA thin films onto a simulated functional surface such as steel and characterization into the long-term durability and corrosion resistance of the material as a way to determine its suitability as a protective coating. Additional elemental doping into the thin films will also be evaluated to determine what positive mechanical and chemical effects they may possess.

Another avenue that was interesting to explore was the CALPHAD that was mentioned previously which could help tremendously with the knowledge of phase transitions of this HEA. As well as more XRD studies to establish more of storehouse of data for this composition. Further nanoindentation and AFM data post corrosion would give a more long-term idea of how this coating would do in a corrosive environment. In short, this study was truly in its infancy and will potentially be one of many on the journey of material engineering.

References

1. Gao, M. C., Yeh, J.-W., Liaw, P. K., & Zhang, Y. (Eds.). (2016). High-Entropy Alloys. https://doi.org/10.1007/978-3-319-27013-5
2. Bi, Linxia, Xiaona Li, Yinglin Hu, Junyi Zhang, Xiao Wang, Xuecheng Cai, Tongde Shen, et al. "Weak Enthalpy-Interaction-Element-Modulated NbMoTaW High-Entropy Alloy Thin Films." Applied Surface Science 565 (November 2021): 150462. https://doi.org/10.1016/j.apsusc.2021.150462.
3. Zhang, Weiran, Peter K. Liaw, and Yong Zhang. "Science and Technology in High-Entropy Alloys." Science China Materials 61, no. 1 (January 2018): 2–22. https://doi.org/10.1007/s40843-017-9195-8.
4. Huang, Shang-Hao. "Slip to Twinning Transition in the Microstructure of CoCrFeMnNi High Entropy Alloy under High Strain Rate Compression." M.S., Drexel University. Accessed March 30, 2022. https://www.proquest.com/docview/1943997800/abstract/CA07CDD3748B4D0EPQ/1.
5. Tsai, K. -Y., M. -H. Tsai, and J. -W. Yeh. "Sluggish Diffusion in Co–Cr–Fe–Mn–Ni High-Entropy Alloys." Acta Materialia 61, no. 13 (August 1, 2013): 4887–97. https://doi.org/10.1016/j.actamat.2013.04.058.
6. Dinardi, Aaron; Capozzoli, Peter; Shotwell, Gwynne (2008). Low-cost Launch Opportunities Provided by the Falcon Family of Launch Vehicles (PDF). Fourth Asian Space Conference. Taipei. Archived from the original (PDF) on 15 March 2012.
7. Dang, Chaoqun, James U. Surjadi, Libo Gao, and Yang Lu. "Mechanical Properties of Nanostructured CoCrFeNiMn High-Entropy Alloy (HEA) Coating." Frontiers in Materials 5 (2018). https://www.frontiersin.org/article/10.3389/fmats.2018.00041.

8. Alvi, Sajid, Dariusz M. Jarzabek, Mojtaba Gilzad Kohan, Daniel Hedman, Piotr Jenczyk, Marta Maria Natile, Alberto Vomiero, and Farid Akhtar. “Synthesis and Mechanical Characterization of a CuMoTaWV High-Entropy Film by Magnetron Sputtering.” ACS Applied Materials & Interfaces 12, no. 18 (May 6, 2020): 21070–79. https://doi.org/10.1021/acsami.0c02156.
9. Dolique, V., A. -L. Thomann, P. Brault, Y. Tessier, and P. Gillon. “Complex Structure/Composition Relationship in Thin Films of AlCoCrCuFeNi High Entropy Alloy.” Materials Chemistry and Physics 117, no. 1 (September 15, 2009): 142–47. https://doi.org/10.1016/j.matchemphys.2009.05.025.
10. Chen, Jian, Xueyang Zhou, Weili Wang, Bing Liu, Yukun Lv, Wei Yang, Dapeng Xu, and Yong Liu. “A Review on Fundamental of High Entropy Alloys with Promising High–Temperature Properties.” Journal of Alloys and Compounds 760 (September 5, 2018): 15–30. https://doi.org/10.1016/j.jallcom.2018.05.067.
11. Feng, X. B., J. Y. Zhang, Y. Q. Wang, Z. Q. Hou, K. Wu, G. Liu, and J. Sun. “Size Effects on the Mechanical Properties of Nanocrystalline NbMoTaW Refractory High Entropy Alloy Thin Films.” International Journal of Plasticity 95 (August 1, 2017): 264–77. https://doi.org/10.1016/j.ijplas.2017.04.013.
12. Liao, Wei-Bing, Hongti Zhang, Zhi-Yuan Liu, Pei-Feng Li, Jian-Jun Huang, Chun-Yan Yu, and Yang Lu. “High Strength and Deformation Mechanisms of Al0.3CoCrFeNi High-Entropy Alloy Thin Films Fabricated by Magnetron Sputtering.” Entropy 21, no. 2 (February 2019): 146. https://doi.org/10.3390/e21020146.
13. Srivatsan, T., and Manoj Gupta. High Entropy Alloys: Innovations, Advances, and Applications, 2020. https://doi.org/10.1201/9780367374426.

14. Tunes, M. A., Vishnyakov, V. M. (2019). Microstructural origins of the high mechanical damage tolerance of NbTaMoW refractory high-entropy alloy thin films. Materials & Design, 170, 107692. https://doi.org/10.1016/j.matdes.2019.107692
15. Khan, N. A., Akhavan, B., Zhou, H., Chang, L., Wang, Y., Sun, L., Bilek, M. M., Liu, Z. (2019). High entropy alloy thin films of alcocrcu0.5feni with controlled microstructure. Applied Surface Science, 495, 143560. https://doi.org/10.1016/j.apsusc.2019.143560
16. Kim, Y. S., Park, H. J., Mun, S. C., Jumaev, E., Hong, S. H., Song, G., Kim, J. T., Park, Y. K., Kim, K. S., Jeong, S. I., Kwon, Y. H., & Kim, K. B. (2019). Investigation of structure and mechanical properties of tizrhfnicuco high entropy alloy thin films synthesized by magnetron sputtering. Journal of Alloys and Compounds, 797, 834–841. https://doi.org/10.1016/j.jallcom.2019.05.043
17. Braeckman, B. R., Misják, F., Radnóczi, G., & Depla, D. (2016). The influence of Ge and in addition on the phase formation of Cocrcufeni High-entropy alloy thin films. Thin Solid Films, 616, 703–710. https://doi.org/10.1016/j.tsf.2016.09.021
18. Braeckman, B. R., Depla, D. (2015). Structure formation and properties of sputter deposited Nbx-cocrcufeni high entropy alloy thin films. Journal of Alloys and Compounds, 646, 810–815. https://doi.org/10.1016/j.jallcom.2015.06.097
19. Braeckman, B. R., Boydens, F., Hidalgo, H., Dutheil, P., Jullien, M., Thomann, A.-L., & Depla, D. (2015). High entropy alloy thin films deposited by magnetron sputtering of powder targets. Thin Solid Films, 580, 71–76. https://doi.org/10.1016/j.tsf.2015.02.070
20. Xia, A., Depla, D., & Franz, R. (2021). Influence of the nitrogen content on the structure and properties of MoNbTaVW high entropy alloy thin films. Journal of Alloys and Compounds, 850, 156740. https://doi.org/10.1016/j.jallcom.2020.156740

21. Romero, R., Makeswaran, N., Naraparaju, R., & Ramana, C. V. (2021). Examination of the Oxidation and Metal–Oxide Layer Interface of a Cr–Nb–Ta–V–W High Entropy Alloy at Elevated Temperatures. Advanced Engineering Materials, 23(8), 2100164. Portico. https://doi.org/10.1002/adem.202100164
22. Kishore Reddy, C., Gopi Krishna, M., & Srikant, P. (2019). Brief evolution story and some basic limitations of high entropy alloys (heas) – A Review. *Materials Today: Proceedings*, *18*, 436–439. https://doi.org/10.1016/j.matpr.2019.07.256
23. An, Z., Jia, H., Wu, Y., Rack, P. D., Patchen, A. D., Liu, Y., Ren, Y., Li, N., & Liaw, P. K. (2015). Solid-solution crcocufeni high-entropy alloy thin films synthesized by sputter deposition. Materials Research Letters, 3(4), 203–209. https://doi.org/10.1080/21663831.2015.1048904
24. El Garah, M., Briois, P., & Sanchette, F. (2022). Recent progress on high-entropy films deposited by Magnetron Sputtering. Crystals, 12(3), 335. https://doi.org/10.3390/cryst12030335
25. Naresh Kaushik, Anoj Meena, Harlal Singh Mali. (2021) High entropy alloy synthesis, characterisation, manufacturing & potential applications: a review. Materials and Manufacturing Processes 0:0, pages 1-25.
26. Sun, S. J., Tian, Y. Z., Lin, H. R., Dong, X. G., Wang, Y. H., Zhang, Z. J., & Zhang, Z. F. (2017). Enhanced strength and ductility of bulk CoCrFeMnNi high entropy alloy having fully recrystallized ultrafine-grained structure. Materials & Design, 133, 122–127. https://doi.org/10.1016/j.matdes.2017.07.054

27. Xin, S. W., Zhang, M., Yang, T. T., Zhao, Y. Y., Sun, B. R., & Shen, T. D. (2018). Ultrahard bulk nanocrystalline VNbMoTaW high-entropy alloy. Journal of Alloys and Compounds, 769, 597–604. https://doi.org/10.1016/j.jallcom.2018.07.331
28. Li, D., Gao, M. C., Hawk, J. A., & Zhang, Y. (2019). Annealing effect for the Al0.3CoCrFeNi high-entropy alloy fibers. Journal of Alloys and Compounds, 778, 23–29. https://doi.org/10.1016/j.jallcom.2018.11.116
29. Geantă, V., Voiculescu, I., Istrate, B., Vrânceanu, D. M., Ciocoiu, R., & Cotruț, C. M. (2018). The Influence of Chromium Content on the Structural and Mechanical Properties of AlCrFeCoNi High Entropy Alloys. International Journal of Engineering Research in Africa, 37, 23–28. https://doi.org/10.4028/www.scientific.net/jera.37.23
30. Ma, S., Xing, J., Yi, D., Fu, H., Zhang, J., Li, Y., Zhang, Z., Liu, G., & Zhu, B. (2011). Effects of chromium addition on corrosion resistance of Fe–3.5B alloy in liquid zinc. Surface and Coatings Technology, 205(21–22), 4902–4909. https://doi.org/10.1016/j.surfcoat.2011.04.101
31. Dong, Y., Zhou, K., Lu, Y., Gao, X., Wang, T., & Li, T. (2014). Effect of vanadium addition on the microstructure and properties of AlCoCrFeNi high entropy alloy. Materials & Design, 57, 67–72. https://doi.org/10.1016/j.matdes.2013.12.048
32. Chen, M.-R., Lin, S.-J., Yeh, J.-W., Chuang, M.-H., Chen, S.-K., & Huang, Y.-S. (2006). Effect of vanadium addition on the microstructure, hardness, and wear resistance of Al0.5CoCrCuFeNi high-entropy alloy. Metallurgical and Materials Transactions A, 37(5), 1363–1369. https://doi.org/10.1007/s11661-006-0081-3

33. Tanji, A., Fan, X., Sakidja, R., Liaw, P. K., & Hermawan, H. (2022). Niobium addition improves the corrosion resistance of TiHfZrNbx high-entropy alloys in Hanks' solution. Electrochimica Acta, 424, 140651. https://doi.org/10.1016/j.electacta.2022.140651

34. Jiang, H., Li, L., Ni, Z., Qiao, D., Zhang, Q., & Sui, H. (2022). Effect of Nb on microstructure and properties of AlCoCrFeNi2.1 high entropy alloy. Materials Chemistry and Physics, 290, 126631. https://doi.org/10.1016/j.matchemphys.2022.126631

35. Pacheco, V., Lindwall, G., Karlsson, D., Cedervall, J., Fritze, S., Ek, G., Berastegui, P., Sahlberg, M., & Jansson, U. (2018). Thermal Stability of the HfNbTiVZr High-Entropy Alloy. Inorganic Chemistry, 58(1), 811–820. https://doi.org/10.1021/acs.inorgchem.8b02957

36. Zhang, M., Zhang, Y. F., Rack, P. D., Miller, M. K., & Nieh, T. G. (2007). Nanocrystalline tetragonal tantalum thin films. Scripta Materialia, 57(11), 1032–1035. https://doi.org/10.1016/j.scriptamat.2007.07.041

37. Kumar, Devesh (2019). Materials-Structure-Property Correlation Of Tungsten Containing High Entropy Alloys (thesis). Malaviya National Institute of Technology, Jaipur.

38. Li, T.-X., Miao, J.-W., Guo, E.-Y., Huang, H., Wang, J., Lu, Y.-P., Wang, T.-M., Cao, Z.-Q., & Li, T.-J. (2021). Tungsten-containing high-entropy alloys: a focused review of manufacturing routes, phase selection, mechanical properties, and irradiation resistance properties. Tungsten, 3(2), 181–196. https://doi.org/10.1007/s42864-021-00081-x

39. Ye, Y. F., Wang, Q., Lu, J., Liu, C. T., & Yang, Y. (2016). High-entropy alloy: challenges and prospects. Materials Today, 19(6), 349–362. https://doi.org/10.1016/j.mattod.2015.11.026

40. Zhang, F., Zhang, C., Chen, S. L., Zhu, J., Cao, W. S., & Kattner, U. R. (2014). An understanding of high entropy alloys from phase diagram calculations. Calphad, 45, 1–10. https://doi.org/10.1016/j.calphad.2013.10.006
41. Feng, X., Zhang, J., Xia, Z., Fu, W., Wu, K., Liu, G., & Sun, J. (2018). Stable nanocrystalline NbMoTaW high entropy alloy thin films with excellent mechanical and electrical properties. Materials Letters, 210, 84–87. https://doi.org/10.1016/j.matlet.2017.08.129
42. Xiao, Y., Zou, Y., Ma, H., Sologubenko, A. S., Maeder, X., Spolenak, R., & Wheeler, J. M. (2019). Nanostructured NbMoTaW high entropy alloy thin films: High strength and enhanced fracture toughness. Scripta Materialia, 168, 51–55. https://doi.org/10.1016/j.scriptamat.2019.04.011
43. Shinde, D., Fritze, S., Thuvander, M., Malinovskis, P., Riekehr, L., Jansson, U., & Stiller, K. (2019). Elemental Distribution in CrNbTaTiW-C High Entropy Alloy Thin Films. Microscopy and Microanalysis, 25(2), 489–500. https://doi.org/10.1017/s1431927618016264
44. Pandey, R. K. (Ed.). (2019). Fundamentals of Electroceramics. https://doi.org/10.1002/9781119057093
45. Behrisch, R. (Ed.). (1981). Sputtering by Particle Bombardment I. Topics in Applied Physics. https://doi.org/10.1007/3-540-10521-2
46. Pharr, G. M., & Oliver, W. C. (1992). Measurement of thin film mechanical properties using nanoindentation. MRS Bulletin, 17(7), 28–33. https://doi.org/10.1557/s0883769400041634

47. Murty, B. S., Yeh, J. W., & Ranganathan, S. (2014). High-Entropy Alloys. High Entropy Alloys, 13–35. https://doi.org/10.1016/b978-0-12-800251-3.00002-x

48. Qiu, Y., Thomas, S., Gibson, M. A., Fraser, H. L., & Birbilis, N. (2017). Corrosion of high entropy alloys. Npj Materials Degradation, 1(1). https://doi.org/10.1038/s41529-017-0009-y

49. Zhao, S., Liu, C., Yang, J., Zhang, W., He, L., Zhang, R., Yang, H., Wang, J., Long, J., & Chang, H. (2021). Mechanical and high-temperature corrosion properties of AlTiCrNiTa high entropy alloy coating prepared by magnetron sputtering for accident-tolerant fuel cladding. Surface and Coatings Technology, 417, 127228. https://doi.org/10.1016/j.surfcoat.2021.127228

50. Dolique, V., Thomann, A.-L., Brault, P., Tessier, Y., & Gillon, P. (2010). Thermal stability of alcocrcufeni high entropy alloy thin films studied by in-situ XRD analysis. Surface and Coatings Technology, 204(12-13), 1989–1992. https://doi.org/10.1016/j.surfcoat.2009.12.006

Vita

Jorge Esding Quezada born July 31st 1995 in El Paso Texas graduated from Bachelors of Mechanical engineering from UTEP in Spring 2020 and Masters of Mechanical engineering fall 2022

Contact Information : <Quezada.esding77@gmail.com>